

Optimistic Verifiable Training by Controlling Hardware Nondeterminism

Megha Srivastava¹ Simran Arora¹ Dan Boneh¹

Abstract

The increasing compute demands of AI systems has led to the emergence of services that train models on behalf of clients lacking necessary resources. However, ensuring correctness of training and guarding against potential training-time attacks, such as data poisoning, poses challenges. Existing works on verifiable training largely fall into two classes: proof-based systems, which struggle to scale due to requiring cryptographic techniques, and “optimistic” methods that consider a trusted third-party auditor who replicates the training process. A key challenge with the latter is that hardware nondeterminism between GPU types during training prevents an auditor from replicating the training process exactly, and such schemes are therefore non-robust. We propose a method that combines training in a higher precision than the target model, rounding after intermediate computation steps, and storing rounding decisions based on an adaptive thresholding procedure, to successfully control for nondeterminism. Across three different NVIDIA GPUs (A40, Titan XP, RTX 2080 Ti), we achieve exact training replication at FP32 precision for both full-training and fine-tuning of ResNet-50 (23M) and GPT-2 (117M) models. Our verifiable training scheme significantly decreases the storage and time costs compared to proof-based systems.

1. Introduction

We are currently in the “large-scale era” of machine learning (ML), where the exciting capabilities of modern AI systems have required a dramatic increase in training compute needs (Sevilla et al., 2022). In turn, several model training services (e.g. Replicate, OpenAI’s Finetuning API, Together AI, Amazon Sagemaker, MosaicML Training) have been created to support clients who lack the resources to train a

¹Department of Computer Science, Stanford University, United States. Correspondence to: Megha Srivastava <megha@cs.stanford.edu>.

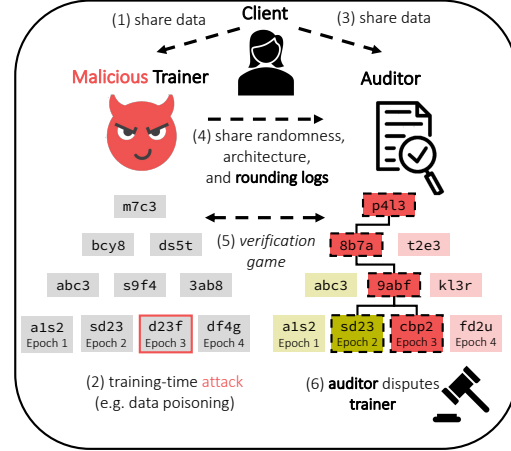


Figure 1. Overview of our verifiable training scheme, based on Deutsch & Reitwießner (2019). After an auditor challenges a trainer on behalf of a client, they train the model themselves, storing weights in a Merkle tree, and enter a binary search procedure to identify the exact steps of the dispute. We show how to account for hardware nondeterminism so that the auditor and trainer can use different GPUs, expanding the pool of potential auditors to any party capable of performing the training task.

model themselves. However, these services require clients to place a significant degree of trust in them to train the model correctly, without any training-time attacks such as data poisoning or undetectable backdoors (Wan et al., 2023; Goldwasser et al., 2022). How can we help a client, who is likely just one individual or a small company, hold the service provider accountable?

Consider an education start-up that wishes to finetune the Llama-70b language model (70B parameters) on their own curated dataset to support student learning. This task requires significant resources, and the company might even lack the necessary expertise. Instead, they might choose to pay a trainer with vast computing resources to perform the training task (Figure 1). However, what if the trainer includes data points that spread misinformation, or introduces backdoors that advance a political agenda only for specific prompts? If the client starts to notice suspicious model behavior, is there any action they can take? We study this problem of *verifiable training*, or ensuring that the training of an ML model was performed correctly.

One possibility is for the the trainer to provide the client a

proof that they did indeed train according to specification. However, proof-based systems require cryptographic techniques that struggle to scale to complexity of real-world ML systems. For instance, recent work based on zero-knowledge proof systems for verifiable *inference*, a much simpler task than training, requires more than 8 minutes to generate proofs for only 20 images (Liu et al., 2021)! Thus, practical proof-based methods for verifiable training have only been implemented for simple tasks such as logistic and linear regression (Garg et al., 2023; Ames et al., 2022).

An alternative “optimistic” approach is to consider a trusted third-party auditor, such as a non-profit organization, that has sufficient compute to perform the training task, even if not at the bandwidth of a service provider (Figure 1). When a client suspects foul play, they can ask the auditor to challenge the trainer by training the model using their own compute, and demonstrate that the trainer did not train correctly. This protocol can be efficiently carried about using techniques from the verifiable computation literature, such as the well-known “verification game” from Deutsch & Reitwießner (2019), which proposes a binary-search procedure to identify the exact intermediate computation steps (e.g. training epochs) that two parties diverge on.

Unfortunately, the issue with such “optimistic” approaches is nondeterminism during model training – two models trained on different GPU types, even with same data ordering and random seed, can learn different weights (Figure 2). The auditor cannot simply compare their model weights with the trainer’s, and recent work has shown that protocols based on comparing model weights, such as Jia et al. (2021)’s “proof of learning,” are non-robust and can be easily forged due to errors from nondeterminism (Thudi et al., 2022; Fang et al., 2023).

We address this limitation by asking: can the trainer provide additional information to the auditor that removes the effects of hardware nondeterminism? Our key insight is that hardware nondeterminism occurs due to the accumulation of errors from floating point operations, and so if we choose to perform computation steps in a *higher* precision (e.g. FP32) than the target precision of the model weights (e.g. FP16), and periodically round back to the target precision, such errors can be “absorbed” by the lower-precision bits. However, because of values that straddle the rounding boundary, it is still possible for the trainer and auditor to round in different directions and diverge. If the trainer also shares rounding directions for every intermediate computation with the auditor (which requires far fewer bits than sharing computation outputs), the auditor can replicate the exact training procedure and eliminate errors due to hardware nondeterminism.

We use this strategy to adapt the verification game described by Deutsch & Reitwießner (2019) for verifiable training.

The game’s efficiency lies in our ability to store hashes of model checkpoints in a Merkle tree instead of the entire model weights due to eliminating nondeterminism error (Merkle, 1988). To determine if training was performed correctly, the auditor only needs to compare the root hash of their Merkle tree with that trainer’s – if they do not match, the two parties can enter an interactive binary search procedure to identify the exact training steps of the dispute. We then show this verifiable training scheme can scale to tasks such as full training of ResNet-50 (23M parameters) and finetuning of GPT-2 (117M parameters), significantly outperforming existing methods with respect to both time and storage cost, while eliminating statistical error due to non-determinism. For example, the proposal in prior work Jia et al. (2021) would require $> 140\times$ more storage cost than our method by saving and comparing model weights at every step in order to achieve the lowest possible (yet still non-zero) statistical error.

Concretely, our contributions include: (1) A novel verifiable training scheme based on the verification game from Deutsch & Reitwießner (2019), which stores model weights in a Merkle tree for efficient comparison between a trainer and auditor; (2) A method for two parties, training the same model on different GPU types, to achieve identical results based on sharing rounding decisions; (3) Experiments showing the ability of our approach to scale to large models such as ResNet-50 and GPT-2 between three different NVIDIA GPU architectures (A40, Titan XP, RTX 2080 Ti); (4) Methods to reduce the storage cost of our approach via efficient encoding of rounding logs and an adaptive threshold mechanism to reduce the amount of rounding decisions logged; and, (5) Comparisons with existing methods, including proof-based systems, that highlight the improved storage and time efficiency of our method.¹

2. Related Works

Attacks on Model Training: Without any verifiable training scheme, significant trust is placed in the trainer. This leaves a client vulnerable to a variety of different attacks, such as “poisoning” of data samples to cause undesirable model behaviors (e.g., generating unsafe, text (Carlini et al., 2023; Koh et al., 2021; Wan et al., 2023)) and planting of hard to detect & remove backdoors triggered by certain inputs (Hubinger et al., 2024; Goldwasser et al., 2022).

Verifiable ML: Training and running inference on ML models in trusted environments has been an exciting direction explored by many researchers. One line of work consists of proof-based systems, where a proof of correctness (for a desired specification) is provided using cryptographic tech-

¹Our method is implemented entirely within the `pytorch` framework, and is available at <https://github.com/megabyte/verifiable-training>.

niques such as succinct zero-knowledge non-interactive arguments (zk-SNARKs) (Micali, 1994; Lee et al., 2020; Liu et al., 2021; Garg et al., 2023; Kang et al., 2022). The majority of these works focus on the easier problem of verifiable *inference*, or proving that a prediction indeed came from a given model. However, such methods require approximations for non-linear functions such as softmax and ReLU activations, and require proof times on the order of minutes for a single data input (Liu et al., 2021). Subsequently, even the most recent proof-based systems for verifiable *training* suffer extreme latency, such as 22 minutes for training VGG-11 on one batch of 16 data inputs (Abbaszadeh et al., 2024), and efficient protocols have only been developed for simple models such as linear and logistic regression, for which we believe it is less likely for a client to delegate out training in the first place (Garg et al., 2023; Ames et al., 2022).

An alternative direction is to consider hardware-based solutions, such as training models in trusted execution environments (TEEs). Such approaches would only require a 3rd-party auditor to review the source code and training data that is used by the trainer and attested for by the TEE, and not perform expensive model training themselves as in our approach. Unfortunately, TEEs such as NVIDIA’s recently announced H100 “Confidential GPU” not only incur a high performance penalty for model training due to the I/O operations required for encrypting training data (Dhanuskodi et al., 2023), but also run the risk of losing all security guarantees if any attacker extracts the attestation key, as has been successfully demonstrated by several previous works (Nilsson et al., 2020; Bulck et al., 2018).

Most similar to our approach are proof-of-learning protocols, which also consider a trust third-party that compares checkpointing during the course of training with the original training sequence (Jia et al., 2021). However, such methods not only incur high storage cost by requiring model weights to be stored frequently, but are subject to statistical error from training nondeterminism. Several works have shown that proof-of-learning protocols can be spoofed and fail to verify correctness in several important contexts, including training tasks such as machine unlearning, where the trainer needs to produce a new model that “forgets” specific training data due to privacy legislation (Fang et al., 2023; Kong et al., 2023; Thudi et al., 2022). Although Choi et al. (2023) recently proposed a verification procedure that is immune to several known proof-of-learning attacks, their method is not only limited to supervised learning algorithms, but also based on an assumption that models temporarily overfit data during training, which may not hold true for all training tasks. Overall, these works argue that the main limitation for provably robust protocols is error due to training nondeterminism, motivating our work.

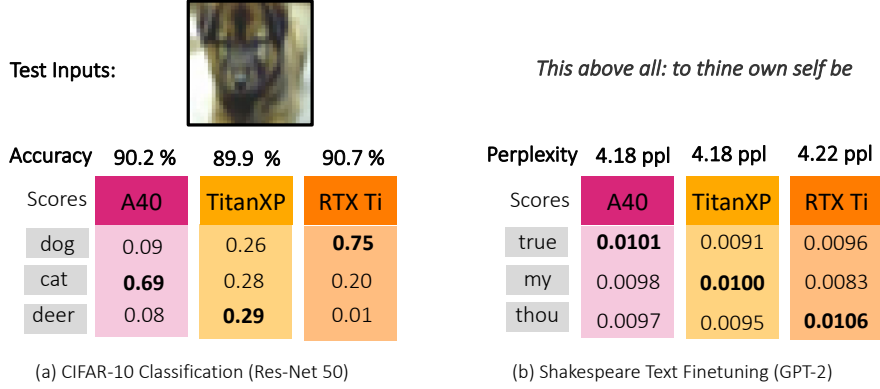
GPU Nondeterminism: Prior work has investigated soft-

ware patches for deterministic training, for instance by enforcing floating point accumulation ordering, at a significant cost to efficiency (Jooybar et al., 2013; Defour & Collange, 2015; Chou et al., 2020; TensorFlow, 2021; Zhuang et al., 2021). However, while these options address the issue of deterministic computation on a *single* GPU architecture — achieving deterministic results across multiple GPU architectures remains challenging (Crane, 2018a; NVIDIA, 2022). Our work seeks to control hardware nondeterminism across architecture types in order to design an efficient and reliable verifiable training scheme. The value of a deterministic training scheme extends beyond verifiable training — researchers have shown that training nondeterminism can have several negative consequences, including concerns of fairness due to causing inconsistent performance on minority subgroups of the data, the reproducibility of published results, and downstream effects on complex ML pipelines (Zhuang et al., 2021; Crane, 2018b; Srivastava et al., 2020).

3. Set-Up: The Verification Game

Our method for verifiable training is based on the interactive verification game proposed by Deutsch & Reitwießner (2019) in the context of blockchains. The basic idea of the verification game is to resolve a dispute between a challenger, in our case the auditor, and a solver, in our case the trainer, for an expensive computation (e.g. model training). In order for the auditor to take any meaningful action (e.g. pursue legal action), they need to prove the exact source of the dispute (e.g. training time-step where an attack occurred). If we can save model weights at different time steps $t = 1 \dots T$ into a compact data structure such as a Merkle tree, then identifying the source of disagreement can be run efficiently via binary search (Merkle, 1988). More formally, the verification game consists of the following parties:

- **trainer**, who has putatively trained a model according to a set of specifications. In our example, this is a service provider (e.g. a large company) with sufficient compute power to train a model on behalf of a client.
- **client**, who receives a model from the trainer and is concerned about its correctness. They are unable to perform the training task themselves, and is willing to share their data with both trainer and auditor.
- **auditor**, who officially challenges the trainer on behalf of a client. This is a trusted 3rd-party that also has sufficient resources to perform the same training task as the trainer, but does not provide such training as a service. While the auditor could be trusted regulatory organization, our work opens up the possibility of the trainer relying on another provider for auditing, leveraging the rapid increase in model training services.
- **judge**: In some cases, it may be desirable to pursue



fixed training data order, software version, and random seed

Figure 2. Even after controlling for the same software version, random seed, and use of nondeterministic algorithms via library flags, training nondeterminism persists between GPU types, posing a challenge for verifying training correctness.

legal action and have a judge arbitrate. The judge can only perform minimal computations (e.g. training for one epoch), but can examine the auditor’s claims and enforce a penalty against either the trainer, for training incorrectly, or the auditor, for raising a false alarm.

When the trainer is approached by an auditor, they would need to share training parameters, model architecture, and randomness, as shown in Figure 1. The auditor would then replicate the training process, storing model weights at the same interval k as the trainer did in a Merkle tree, which is a tree where every leaf node is a hash of the model weights and every non-leaf node is a hash of its children nodes. The main loop of the verification game starts when both parties have the root hash of their respective Merkle trees – if training was performed correctly, then the trainer’s root should match the auditor’s. Otherwise, a binary search procedure is performed, where the auditor iteratively descends the data structure until it identifies two consecutive leaf nodes, i and $i + 1$, where the hash at i matches that of the trainer, but not $i + 1$, thereby identifying the source of the dispute.

Overall, this interaction requires cooperation with the trainer – for example, if a trainer refuses to share the value at a certain node of their Merkle tree within a given time frame, they can be considered to have failed the audit. Additionally, we emphasize that the trainer and auditor can only use an efficient Merkle tree structure to store model weights, requiring far less storage than prior work, if correct training produces identical weights (and therefore identical hash values). Unfortunately, training nondeterminism between GPUs leads to weight divergence, which is why we seek to control it.

4. The Nondeterminism Challenge

Although there exist user-side controls for deterministic operations within a single GPU architecture (e.g. NVIDIA

H100), these controls do not prevent nondeterminism between GPU architectures (e.g. NVIDIA H100 and V100), where trained models can have similar aggregate performance (e.g. accuracy) yet yield very different predictions (Figure 2) (Crane, 2018a; NVIDIA, 2022). We now briefly discuss the source of nondeterminism between GPU types.

Floating Point Arithmetic: Computers represent real values using integer and floating-point representations, typically using the IEEE 754 standard (Figure 3). There is a tradeoff between the approximation fidelity and the # of bits used to represent the real values. The chosen precision controls the representable numerical range (e.g. 32-bit floating-point values can represent values between $1.17549435e-38$ and $3.40282347e+38$). Because computers round to representable floating point values, changing the order in which floating point numbers are accumulated can change the resulting sum (Kahan, 1965; Whitehead & Fit-Florea, 2011).

Example: Floating Point Addition Consider three values $a = 0.1$, $b = -0.1$ and $c = 0.2$ in FP32. The following two orders of summation — $a + c + b$ vs. $a + b + c$ yield different results — 0.200000017881 vs. 0.200000002980.

Over the course of the many operations involved in training, rounding can lead to large differences in end results.

Parallel Computation: In GPUs a single operation (called a *kernel*) is executed by 1000s of threads in parallel. In NVIDIA terminology, GPUs contain a set of *streaming multiprocessors* (SMs), which run the *thread blocks* required for the kernel. At the hardware level, the blocks are divided into *warps*, or groups of threads, that are assigned to the available cores. Applications partition arithmetic workloads (e.g. batch matrix multiplies), differently depending on the GPU architecture to achieve high performance (NVIDIA, 2022), thus changing the order of floating point operations. Different GPUs have different # and sizes of compute units — for instance, the number and tile dimensions of tensor

| Example | Summation Order | FP32 | FP32 Rounded to FP16 |
|--|-----------------|----------------------------------|----------------------|
| $a, b, c = 0.1, -0.1, 0.2$ | $a + b + c$ | 00111110010011001100110011001101 | 0011001001100110 |
| | $a + c + b$ | 00111110010011001100110011001110 | 0011001001100110 |
| $a, b, c = 10.02, 13.162813186645508, 0.2$ | $a + b + c$ | 01000001101110110001000000000001 | 0100110111011001 |
| | $a + c + b$ | 01000001101110110001000000000000 | 0100110111011000 |

Table 1. Two examples of floating point accumulation error when rounding arithmetic performed higher precision (e.g. FP32) down to lower precision (e.g. FP16). In the first example, error in the FP32 result *does not* transfer to the rounded FP16 result. In the second example, the error in the FP32 result *does* transfer to the rounded result.

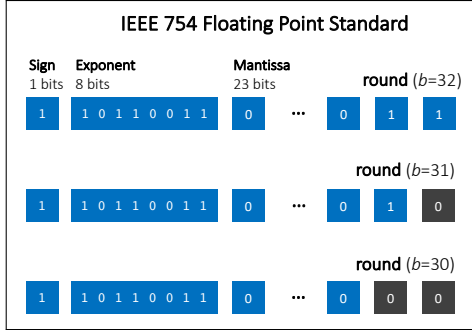


Figure 3. We define rounding to b bits as rounding to the nearest 32-bit floating point that has 0s in the last $32 - b$ bits of the mantissa, after accounting for the exponent.

core units (specialized matrix multiplication units on the GPU) across NVIDIA Volta and Turing vs. Ampere and Hopper architectures varies (Sun et al., 2022).

Memory Hierarchy and Variable Delays: The time taken for memory access by each thread depends on the physical location of the data, which can create variable delays (Jooybar et al., 2013; Defour & Collange, 2015; Chou et al., 2020). In accessing data, the GPU memory hierarchy consists of large amounts of high bandwidth memory (HBM) and small amounts of fast SRAM memory allocated to each SM, and maintains an L1 and L2 cache to improve access times for reused data. The caches sizes and access times differ across GPU architectures, which affects warp scheduling. For instance, an NVIDIA A100 has 192KB / 40 MB of L1 and L2 cache memory respectively, while the H100 has 256KB / 50MB respectively (NVIDIA, 2023). Further, the physical locations of individual SMs differ in distance from the cache and HBM memory on chip.

Non Determinism To compute primitives such as GEMMs ($D = AB + C$), the workhorse of machine learning, GPUs split the work of computing the tiles of D across a thread block (NVIDIA, 2023). The results across threads are accumulated. Due to the varied parallelization and data access patterns across architectures, and the fact that floating point addition is not associative, results across GPU architectures are nondeterministic (Crane, 2018a; NVIDIA, 2022).

Any exact verifiable training method, that does not introduce statistical error, would need to control these sources of nondeterminism across GPU types.

5. Method Overview

Here we provide our method for the verification game in Section 3 (Teutsch & Reitwießner, 2019). We (1) provide our approach for handling nondeterminism from floating point accumulation, (2) provide the algorithms for the trainer and auditor to verify training, and (3) discuss two strategies for storage cost reduction.

5.1. Accumulation Errors Start at Higher Precision Bits

Our key idea is that if nondeterminism of training between GPU types occurs due to floating-point operations, then any error will initially be introduced in the lower bits. Therefore, if both trainer and auditor train at a *higher* floating-point (e.g. $b_{tr} = 64$) precision than the client’s target model precision (e.g. $b_m = 32$) and then periodically *round* (e.g. $b_r = 32$) after intermediate computation steps (e.g. a convolution layer, if operating on a per-layer abstraction such as), they can help “erase” any errors from accumulating due to nondeterminism. Table 1 (Row 1) provides a toy example of how error in higher precision arithmetic is erased when rounding the result to lower precision.

Unfortunately, simply rounding to the nearest FP32 after each computation during training is not sufficient for eliminating nondeterminism due to divergence spanning the *rounding boundary*. Consider Case A in Figure 4, which shows a divergence in the output of a computation using FP64 on two different GPUs. Because the outputs of GPU 1 and 2 are on different sides of the boundary, rounding to the nearest FP32 results in rounding to different values, introducing error. Table 1 (Row 2) provides a toy example of how error in higher precision arithmetic might transfer to the lower precision rounded result.

What if the trainer records their rounding choice (e.g. up, down, none) for every intermediate computation? The auditor could then copy the *trainer’s* choice, and therefore round to the exact same value and successfully control for nondeterminism. However, as we show in Case B in Figure 4, the auditor should not copy the trainer’s behavior for every output. If a computation output on GPU 1 is too close to the rounded value, then it is possible that GPU 2 is also close in distance but from the opposite direction – in this case, the auditor should ignore the trainer’s choice.

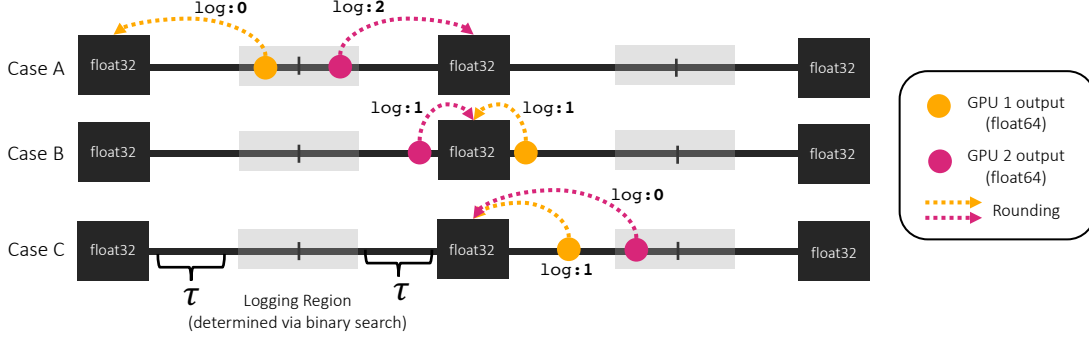


Figure 4. Divergence between outputs on two different GPU types (in FP64) for a given function and input can result in different rounding choices when rounding to the nearest FP32. We only wish to log rounding decisions for situations like Case A, where the auditor should copy the trainer’s rounding choice in order to reach the same value. This requires defining a logging region, determined by a threshold τ ,

We therefore need to introduce a threshold τ under which the trainer does not record their rounding choice.

The success of this method relies on our ability to upper bound the divergence d_{div} between any two different GPUs for any intermediate computation f (i.e. difference in outputs for the same input). Let ϵ_b represent the distance between two FP32 values, after rounding to b_r bits of the mantissa (Figure 3) and controlling for the exponent. We need to select b_r and τ such that $d_{div} < \epsilon_{b_r}$ and $d_{div} < 2\tau$ (Figure 4). Because the set of possible floating point numbers is finite, there do exist optimal bounds for b_r and τ – in practice, we find that $b_r \leq 32$ and $\tau > 0.25 * \epsilon_{32}$ are sufficient for standard intermediate computations in neural network training (e.g. convolution, layer norm) in FP64, and experiment with different values for b_r in Section 6.

We next discuss the specific functions our method requires, algorithm details for both the trainer and auditor, and our approach for reducing storage cost.

Algorithm 1 log

INPUT: value x , rounding amount b_r , threshold τ , file F

- 1: $\text{exp} \leftarrow \text{get exponent of } x$
- 2: **if** $|x - \text{rnd}_{b_r}(x)| > \text{exp} * \tau$ **and** $x < \text{rnd}_{b_r}(x)$ **then**
- 3: $\text{write}(2, F)$ // log rounding up
- 4: **else if** $|x - \text{rnd}_{b_r}(x)| > \text{exp} * \tau$ **and** $x > \text{rnd}_{b_r}(x)$ **then**
- 5: $\text{write}(0, F)$ // log rounding down
- 6: **else**
- 7: $\text{write}(1, F)$ // log rounding ignore
- 8: **end if**

5.2. Primitives

Our work assumes both trainer and auditor train models using the IEEE-754 standard for floating-points (Figure 3). In addition to requiring read and write disk I/O operations, we define the following functions:

Algorithm 2 train

INPUT: dataset D , epochs E , batch size B , shared randomness R , model W_θ , loss function loss , rounding amount b_r , training precision b_{tr} , target model precision b_m , checkpointing interval k

OUTPUT: Merkle tree root M_{root} , rounding log file F

- 1: $F, M_{leaves} \leftarrow \text{create empty file and leaf list}$
- 2: $W_\theta \leftarrow \text{init}(R, b_{tr})$ // initialize weights
- 3: $T \leftarrow \frac{D * E}{B}$
- 4: **for** $t = 1 \dots T$ **do**
- 5: $\text{input} \leftarrow \text{batch}(R, D, B)$ // get data batch
- 6: // forward pass
- 7: **for** layer $l_\theta \in W_\theta.\text{layers}$ **do**
- 8: $\text{output} \leftarrow l_\theta(\text{input})$
- 9: $\tau \leftarrow \text{threshold}(l_\theta, b_r, b_{tr})$ // set threshold
- 10: $\text{log}(\text{output}, b_r, \tau, F)$
- 11: $\text{output} \leftarrow \text{rnd}_{b_r}(\text{output})$
- 12: $\text{input} \leftarrow \text{output}$
- 13: **end for**
- 14: $\text{loss} \leftarrow \text{loss}(\text{output})$
- 15: // backward pass, reversed layers
- 16: $\text{grad_output} \leftarrow \nabla_{\text{loss}}$
- 17: **for** layer $l_\theta \in W_\theta.\text{layers}$ **do**
- 18: $\text{grad_input} \leftarrow \nabla_{l_\theta}(\text{grad_output})$
- 19: $\tau \leftarrow \text{threshold}(\nabla_{l_\theta}, b_r, b_{tr})$
- 20: $\text{log}(\text{grad_input}, b_r, \tau, F)$
- 21: $\text{grad_input} \leftarrow \text{rnd}_{b_r}(\text{grad_input})$
- 22: $\text{grad_output} \leftarrow \text{grad_input}$
- 23: **end for**
- 24: $\theta \leftarrow \text{update update weights}$
- 25: **if** $t \bmod k = 0$ **then**
- 26: $M_{leaves}.\text{append}(\text{hash}_{\text{sha256}}(\theta \text{ in precision } b_m))$
- 27: **end if**
- 28: $M_{root} \leftarrow \text{tree}(M_{leaves})$ // create Merkle tree
- 29: **return** F, M_{root} , and model W_θ in target precision b_m

1. $\text{rnd}_{b_r}(x)$: rounds input x to the nearest float up to b_r bits of the mantissa, as shown in Figure 3.
2. $\text{log}(x, b_r, \tau, f)$: logs to file f a logging direction c , which is either 0 (down), 1 (ignore), or 2 (up) depending on threshold τ and rounding amount b_r , as shown in Algorithm 1.
3. $\text{rev}(x, b_r, c)$: reverses rounding of input x based on logging direction c . If $x < \text{rnd}_{b_r}(x)$ and $c = 0$, then return x rounded to the nearest float *below* x with b_r precision. If $x > \text{rnd}_{b_r}(x)$ and $c = 2$, then return x rounded to the nearest float *above* x with b_r precision. Otherwise, do not correct.
4. $\text{threshold}(l, b_r, b_{tr})$: identifies the optimal threshold to log rounding directions (0 or 2) instead of 1, which the rev function ignores, based on a binary search procedure described in Section 5.5.
5. $\text{hash}_{\text{sha256}}(\theta)$: creates a SHA-256 hash of provided model weights θ via serialization. The model weights should be in the client’s target precision $b_m < b_{tr}$.
6. $\text{tree}(\text{leaf}_1, \text{leaf}_2, \dots, \text{leaf}_n)$: create a Merkle tree by repeatedly hashing pairs of nodes until one hash remains (Merkle, 1988). In our work, each *leaf* node is the output of $\text{hash}_{\text{sha256}}(\theta)$ for model weights θ at a given checkpoint, with a checkpointing interval k .

5.3. Trainer

The trainer’s task begins when a client approaches them with dataset D , training specifications (epochs E , loss function loss, etc.), and a requested model precision b_m . The trainer can then choose a training precision $b_{tr} > b_m$, a rounding amount $b_r \leq b_m$, and a checkpointing interval k to periodically store small $\text{hash}_{\text{sha256}}(\theta)$ of model weights θ in a Merkle tree, for efficient comparison with an eventual auditor. Then, as detailed in Algorithm 2, the trainer can perform training as normal, but after every intermediate computation (e.g. convolution) perform the rnd_{b_r} operation on each output. Rounding is applied to computations in both the forward and backward passes. Finally, either using a fixed threshold τ or a layer-specific optimal τ from the threshold function described in Section 5.5, the trainer applies log, which logs rounding choices *only for the computations an auditor should copy*. The output of the algorithm includes a rounding log file F and the root of the Merkle tree which, along with the shared randomness R and all training parameters, the trainer can share with any trusted third-party auditor who challenges them.

5.4. Auditor

After a client approaches them (and shares their data), the auditor can initiate the verification game described in Section 3. To avoid facing a penalty, the trainer must cooperate by sharing the chosen rounding amount b_r , randomness R used in training (e.g. a pseudo-random number generator),

details of the model architecture and training parameters, the checkpointing interval k , and set of rounding logs F . The auditor then follows the training procedure and corrects their rounding choice (e.g. up or down) to match those logged in F using the rev operation, as detailed in Algorithm 3 in the Appendix. By correcting for each rounding choice mismatch with the trainer during the course of training, the auditor is able to prevent errors due to nondeterminism to accumulate. Therefore, the auditor can store the $\text{hash}_{\text{sha256}}(\theta)$ of model weights θ in a Merkle tree at interval k , knowing that if training was done correctly, the model weights should be identical to the trainer’s at any timestep. The output of Algorithm 3 is the root of the auditor’s Merkle tree, which they can use to compare with the trainer’s root.

5.5. Reducing storage cost

Logging rounding decisions for every neural network layer output during training incurs a large baseline storage cost, and is the main limitation of our work. More formally, for dataset D , batch size B , number of training epochs E , and model layers L_θ , the upper bound on the total storage cost for verifiable training with our method is:

$$\text{storage cost (B)} = |D| * E * B * \left(\sum_{l=1}^L o_{l,f} + \sum_{l=1}^L o_{l,b} \right) \quad (1)$$

where $o_{l,f}$ and $o_{l,b}$ represent the size of outputs of the forward pass and backward pass of layer l . Note that the log entries do not need to be kept around in the RAM and can be written straight to the disk. Moreover, this cost is a one-time cost incurred by the trainer, who in our context is likely to be a powerful commercial provider with access to such storage capacity. Furthermore, as we later show in Section 6, for models with many linear layers like Transformer-based language models (e.g. GPT-2), where parameters significantly outnumber intermediate computations, this storage cost is significantly smaller than alternative approaches that require saving model weights (Jia et al., 2021). Nevertheless, we now describe our method for reducing storage cost by (i) efficiently encoding rounding logs and (ii) adaptive selection of the threshold τ to reduce the storage costs.

Efficient Encoding: Recall that $\text{log}(x)$ only logs one of three possible values from the set 0, 1, 2, as opposed to the floating point model weights. We pack sub-sequences of five log entries into a single byte via a fast GPU-based radix-3 to radix-2 conversion, yielding 1.6 bits/entry storage that is close to the best possible packing of 1.58 bits/entry, and yields a 77% storage reduction in practice relative to naively storing one log entry per byte.

Adaptive Threshold: Recall that we need to select a threshold τ that controls for whether the trainer logs a rounding choice, or instead logs 1 which the auditor ignores. The

more one can increase τ , the more 1 values are recorded which, if significant, can make the rounding more compressible (due to an increase in long sequences of 1s). Furthermore, it is possible that the divergence d_{div} between outputs on two different GPUs, given the same input, is function-specific. For example, while the convolution operation requires several matrix multiplications that might result in large floating point accumulation error, operations such as scaling are unlikely to result in large d_{div} , and a larger τ can be applied. We develop an efficient algorithm (Algorithm 4 in the Appendix) to find the optimal value for τ given a particular layer and data of output values that led to different rounding choices between any two GPUs (e.g. Case A in Figure 4). For a given rounding amount b_r and training precision b_{tr} , the algorithm performs a binary search between $\tau = 0.25 * \epsilon_{32}$ (our assumed upper bound for the d_{div} between two GPUs for any function) and $\tau = 0.5 * \epsilon_{b_r}$ (the rounding boundary). By performing this procedure for the different intermediate computations in a model, the trainer can hope to log more values of 1, leading to a stronger compression of the rounding log F .

Merkle Tree Storage: The only other additional storage required of our method is the Merkle tree of model checkpoints (which is negligible compared to the rounding logs). Storing SHA-256 hashes of model weights during training in a Merkle tree creates an efficient mechanism for the verification game described in Section 3, and the audit ends when either the trainer withdraws, the auditor confirms that training was performed correctly, or the auditor can present paths to the two leaves of their Merkle tree where the training runs first started to diverge, thereby providing evidence to dispute the trainer. Comparing two Merkle trees given their root hash is a standard binary search procedure.

6. Empirical Results

We evaluate our verifiable training method on the two large-scale models listed below with all possible trainer and auditor pairs across the following three NVIDIA GPU architectures: A40, TITAN Xp, and RTX 2080 Ti (see Appendix Section A for more details). Additionally, in Section 6.4, we compare our method with a proof-based system for logistic regression as no known proof-based systems exist for the large-scale models we have considered.

1. **ResNet-50:** We train (from random initialization) ResNet-50 (23M) on CIFAR-10 with dataset size 50,000 and batch size $B=64$. Training for 100 epochs results in test accuracy of 90.7% on a Titan RTX Ti.
2. **GPT-2:** We finetune GPT-2 (117M) on a corpus of Shakespeare text with dataset size 1.1M tokens, batch size $B=8$, and sequence length 64. Training for 1 epoch results in perplexity 4.22 on a Titan RTX Ti.

In Figure 2 we show that nondeterminism due to GPU architecture exists for both training tasks – while using library flags and deterministic settings allow us to repeatedly obtain identical results across training runs on the same GPU architecture, training on different GPU architectures results in fundamentally different models.

6.1. Implementation details

We implement our verifiable training method entirely on top of the pytorch framework, with torch version 1.13.1 and CUDA version 11.7. The intermediate computations we apply `rnd_b` to are layers (e.g. `torch.nn.Conv2D`) in the model’s computation graph. Rounding-related operations (`rnd` and `rev`) either using casting or floating-point functions (e.g. `torch.nextafter`) that can run on the GPU, thus having little impact on computational speed. Because we observed that the `torch.randn` operation used for dropout in GPT-2 is non-deterministic for long inputs (even for the same seed, see Appendix E), we implement our own dropout as our method requires shared randomness R .

6.2. Successful control for non-determinism

Our method completely eliminates non-determinism between full training runs of both for both the ResNet-50 training and GPT-2 fine-tuning tasks across all possible trainer and auditor pairs between the A40, Titan XP, and RTX 2080 Ti GPUs. As Figure 5 shows, standard FP32 training results in an increasing divergence (l2-distance of weights) between models on different GPUs over the course of training. Furthermore, we show the simple approach of training in FP64 and rounding to FP32 after every intermediate computation, but without the auditor correcting rounding decisions with `rev`, fails to mitigate this issue. Only our method, in which the auditor follows the rounding decisions ($b_r = 32$) made by the trainer for every intermediate computation, eliminates non-determinism and persists over time.

Our implementation, which requires disk I/O during training to store the rounding decisions, results in a small increase in training time for the trainer (1.2-1.4x) and auditor (1.3-1.7x) using a non-optimized, prototype implementation (Table 5). We report the storage requirements of our method in Table 2, showing that our efficient encoding scheme reduces the size of the trainer’s rounding logs by 77%, relative to naive logging. Because the Merkle tree stores 32-byte SHA-256 hashes, its overall size (KBs) and creation time are negligible and not reported.

Finally, we show that decreasing the rounding amount b to values even as low as 26 has little effect on model performance (we observe no change in accuracy, so report test loss), but increase training time (Figure 5). We observe that smaller values of b do allow more log entries to be ignored,

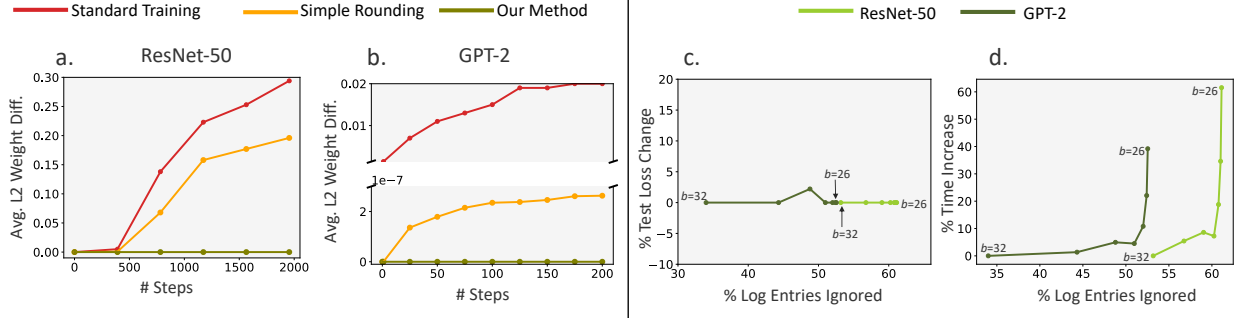


Figure 5. We successfully control for nondeterminism between GPU types for both ResNet-50 (a.) and GPT-2 (b.) tasks, while standard training and simple rounding without performing rev corrections result in model divergence over the course of training. Stronger rounding has minimal affect to model performance (c.), but at the cost of increasing time for trainer (d.).

Table 2. Efficient encoding reduces storage requirements by 77%, and rounding to $b = 26$ improves the compression further between 5-20% (values reported for 1 step of training). The original proof-of-learning protocol from Jia et al. (2021) requires storing 2.78 GB of model weights for GPT-2, or more than **140x** our storage cost, while still incurring statistical error.

| | ResNet-50 $b = 32$ | ResNet-50 $b = 26$ | GPT-2 $b = 32$ | GPT-2 $b = 26$ |
|--------------------|--------------------|--------------------|----------------|----------------|
| Naive Encoding | 456 MB | 456 MB | 92 MB | 92 MB |
| Efficient Encoding | 105 MB | 105 MB | 22 MB | 22 MB |
| + Zip Compression | 96 MB | 91 MB | 20 MB | 18 MB |

improving compression of the file, which we discuss next.

6.3. Compression with adaptive threshold

Our approach particularly outperforms (Table 2) the storage costs of proof-of-learning protocols that save model weights for GPT-2 (2.78GB), which has many linear layers – we observe more than **140x** reduction relative to the approach in Jia et al. (2021). We further reduce the storage cost of our method by decreasing the rounding amount b and implementing the adaptive thresholding strategy (Section 5.5).

In Table 4, we report adaptive thresholds τ for 4 different pytorch layers at rounding amount $b_r = 32$. Convolutions require the lowest τ , indicating larger divergence in outputs between GPU types, which is expected due to the large number of matrix multiplications. Meanwhile, τ is higher for normalization layers, likely due to smaller divergences between GPU types. Because adaptive thresholding seeks to reduce the number of times rounding decisions (0 and 2) are logged and improve log file compression, we report storage cost after zip compression in Table 2. As expected, more aggressive rounding (which results in a higher τ) improves the compression rate. Although the compression gains are mild in comparison to our encoding step, such differences build-up over the course of training.

Finally, we report the average # of rev corrections an auditor needs to perform for one training step in our two tasks (Table 3). These values are surprisingly small in comparison to the number of operations logged – only a maximum of 25, or **2e-6%** (ResNet-50) and **9e-6%** (GPT-2) of

logged values, are actually needed by the auditor! We also observe that severe rounding (e.g. $b = 27$) completely eliminated the hardware non-determinism for our tasks, requiring no corrections from the auditor. This shows a huge gap between the # of values currently saved by the trainer and those actually needed by the auditor. An exciting direction for future work, therefore, is to develop methods that could reliably predict when a divergence will not occur and skip logging entirely, reducing the overall storage cost of our method.

6.4. Comparison with alternative approaches

Logistic Regression Garg et al. (2023) recently proposed a zero-knowledge proof-based system for verifiable training of a logistic regression, which importantly does not leak information about the client’s data or require a trusted third-party auditor, unlike our work. However, since verifiable training itself is motivated by a client not having sufficient resources to train the model, it is crucial to consider the implications of scale. The authors report the prover time and proof size requirements for one training pass of logistic regression on a dataset of 2^{18} items, with 1024 dimensions and a batch size of 2014, as **72 seconds** (training and proof generation time) and **350 MB** respectively. We replicate this training task, and find that our method significantly improves upon both storage and time requirements, requiring only **106 KB** and **7 seconds** (both training and auditing). Furthermore, because Garg et al. (2023) do not report the duration of “offline phase” of their method, their reported value is a lower bound on the actual time required. Finally, we note that the original proof-of-learning protocol from

Table 3. Average number of rev corrections performed by auditor per step of training. Even at $b = 32$, the auditor only makes 20-25 corrections (**2e-6 to 9e-6%** of samples) per training step, suggesting significant opportunity for reducing the storage cost of our method.

| ResNet-50 | $b = 32$ | $b = 31$ | $b = 30$ | $b = 29$ | $b = 28$ | $b = 27$ | $b = 26$ |
|------------------|--------------|----------------|---------------|---------------|---------------|-----------|-----------|
| Forward | 15 ± 3 | 6 ± 2 | 3 ± 1 | 3 ± 1 | 0 | 0 | 0 |
| Backward | 10 ± 0.6 | 6 ± 0.6 | 2 ± 1 | 0.7 ± 0.7 | 0 ± 0 | 0 ± 0 | 0 ± 0 |
| GPT-2 | $b = 32$ | $b = 31$ | $b = 30$ | $b = 29$ | $b = 28$ | $b = 27$ | $b = 26$ |
| Forward | 2 ± 0.7 | 2.3 ± 0.8 | 2.2 ± 0.4 | 0.2 ± 0.2 | 0.4 ± 0.2 | 0 ± 0 | 0 ± 0 |
| Backward | 19 ± 13 | 0.75 ± 0.3 | 1.2 ± 0.4 | 0.2 ± 0.2 | $0. \pm 0.0$ | 0 ± 0 | 0 ± 0 |

Table 4. Adaptive thresholds identified for different operations using the binary search procedure from Algorithm 4 with $b = 32$.

| | 2D Convolution | Batch Norm | Linear | Layer Norm |
|-----------|-----------------------|--------------------|-------------------|-------------------|
| Dimension | 256 (1,1) | (128, 128, 16, 16) | (768,768) | (768,1) |
| τ | $0.305 * 2^{-23}$ | $0.499 * 2^{-23}$ | $0.465 * 2^{-23}$ | $0.499 * 2^{-23}$ |

Jia et al. (2021), which also considers a trusted third-party, would require **9.2 MB per training step** to store all model weights, and therefore our method is the most space efficient by a factor of at least **85x**.

VGG-11 Concurrent to our work, Abbaszadeh et al. (2024) introduce a zero-knowledge proof-of-training protocol for deep neural networks, presenting results for one batch step of training for a simplified version of the VGG-11 model with 10M parameters, which is less than the original VGG-11 network and ResNet-50 (Simonyan & Zisserman, 2015). While the authors unfortunately do not provide the exact details of the simplified architecture, we can assume that increasing the number of parameters to the original VGG-11 would only increase their reported proof time and size. We therefore compare their reported values with an implementation of our method for the same task of verifying training of VGG-11 on CIFAR-10 with a batch size of 16. While their use of incrementally verifiable computation leads to tractable proof size (1.36MB vs. the 1.2MB per iteration cost of our method), Abbaszadeh et al. (2024)’s method requires **22 minutes per training iteration**. In comparison, our method requires training and auditing times of only 6 seconds per iteration, and is thus more efficient by a significant factor of **220x**, which is an important consideration when model training is provided as a commercial service.

Secure GPT-2 Inference The previously discussed proof-based systems for verifiable training by-pass the need for a third-party auditor, but very few efficient systems exist in the literature. Many more works study secure *inference* of deep neural networks, which could be used to construct verifiable training protocols with stronger security guarantees than ours (e.g., allowing a trainer to keep a proprietary model’s weights private), but come at a significant cost to performance and resources. To demonstrate this, we consider adapting Gupta et al. (2023)’s protocol for secure inference of GPT-2 based on multi-party computation, to our context of verifiable training. Gupta et al. (2023) show

how two parties, the client with private data and the trainer, can jointly compute the forward pass of a known model architecture without revealing additional information beyond the model output to each other. Because they report the the communication overhead $P = 0.37\text{GB}$ and time $T = 0.96$ seconds for one forward pass on a single data input, we can calculate $2 \times P \times D \times E = \mathbf{189\ GB}$ and $2 \times T \times D \times E = \mathbf{983\ seconds}$ as estimated communication cost and time, respectively, for 1 step of training in our GPT-2 task, where 2 considers both the forward and backward pass. Compared with our method’s required storage cost (18MB) and training time (11s for training, 13.5 seconds for auditing), scaling Gupta et al. (2023)’s protocol for training would introduce around a **10,000x** data and **40x** time overhead.

We acknowledge that the previous comparisons are not straightforward, as they focus on providing strong security guarantees that do not require a trust third-party. However, this comes at the cost of relying on cryptographic techniques that are difficult to scale, and approximating non-linear functions (e.g. softmax in Transformer attention). By highlighting the trade-offs such methods provide, we hope to motivate future verifiable training schemes that, if one is willing trust a third-party auditor, are more practical for real-world training tasks.

7. Limitations & Future Work

Our efficient scheme for verifiable training successfully controls for hardware nondeterminism and expands the pool of potential auditors of a model training service, allowing us to envision a world where a client can even use two competing service providers it trusts to audit each other. However, one main limitation of our work in comparison with proof-based systems is the need for all parties to trust this third-party *auditor*. If the *trainer* is providing finetuning services on top of models that are not open-source (e.g. OpenAI), then our scheme will only work for the third-

party auditors that the *trainer* is willing to share their model weights.

Another limitation of our work is the storage cost. While we have shown that it is significantly smaller than alternative methods, the vast majority of stored rounding decisions are not used by the *auditor* and are therefore unnecessary (Section 6). Therefore, an exciting direction for future work is to figure out how to mitigate this gap by better predicting when divergence between GPU computations occurs – recent work has similarly argued that a stronger profile of noise during the training process is necessary for robust verifiable training (Fang et al., 2023). Finally, other directions for future work also include adapting our method for distributed training, as well as considering adversarial manipulation of the rounding logs by the *trainer*.

8. Acknowledgements

We would like to thank Bill Dally and Duncan Riach for a helpful discussion at the early stage of the project. Megha Srivastava was supported by an IBM PhD Fellowship and the NSF Graduate Research Fellowship Program under Grant No. DGE-1656518. In addition, this work was funded by NSF, DARPA, the Simons Foundation, UBRI, and NTT Research. Opinions, findings, and conclusions or recommendations expressed in this material are those of the authors and do not necessarily reflect the views of DARPA.

References

- Abbaszadeh, K., Pappas, C., Papadopoulos, D., and Katz, J. Zero-knowledge proofs of training for deep neural networks. Cryptology ePrint Archive, Paper 2024/162, 2024. URL <https://eprint.iacr.org/2024/162>. <https://eprint.iacr.org/2024/162>.
- Ames, S., Hazay, C., Ishai, Y., and Venkitasubramanian, M. Liger: Lightweight sublinear arguments without a trusted setup. Cryptology ePrint Archive, Paper 2022/1608, 2022. URL <https://eprint.iacr.org/2022/1608>. <https://eprint.iacr.org/2022/1608>.
- Bulck, J. V., Minkin, M., Weisse, O., Genkin, D., Kasikci, B., Piessens, F., Silberstein, M., Wenisch, T. F., Yarom, Y., and Strackx, R. Foreshadow: Extracting the keys to the intel SGX kingdom with transient Out-of-Order execution. In *27th USENIX Security Symposium (USENIX Security 18)*, pp. 991–1008, Baltimore, MD, August 2018. USENIX Association. ISBN 978-1-939133-04-5. URL <https://www.usenix.org/conference/usenixsecurity18/presentation/bulck>.
- Carlini, N., Jagielski, M., Choquette-Choo, C. A., Paleka, D., Pearce, W., Anderson, H., Terzis, A., Thomas, K., and Tramèr, F. Poisoning web-scale training datasets is practical, 2023.
- Choi, D., Shavit, Y., and Duvenaud, D. Tools for verifying neural models’ training data. In *Neural Information Processing Systems*, 2023.
- Chou, Y. H., Ng, C., Cattell, S., Intan, J., Sinclair, M. D., Devietti, J., Rogers, T. G., and Aamodt, T. M. Deterministic atomic buffering. In *2020 53rd Annual IEEE/ACM International Symposium on Microarchitecture (MICRO)*, 2020.
- Crane, M. Questionable answers in question answering research: Reproducibility and variability of published results. *Transactions of the Association for Computational Linguistics*, 6:241–252, 2018a. doi: 10.1162/tacl.a.00018. URL <https://aclanthology.org/Q18-1018>.
- Crane, M. Questionable answers in question answering research: Reproducibility and variability of published results. *Transactions of the Association for Computational Linguistics*, 6:241–252, 2018b. doi: 10.1162/tacl.a.00018. URL <https://aclanthology.org/Q18-1018>.
- Defour, D. and Collange, C. Reproducible floating-point atomic addition in data-parallel environment. In *Proc. of the Federated Conference on Computer Science and Information Systems*, 2015.
- Dhanuskodi, G., Guha, S., Krishnan, V., Manjunatha, A., Nertney, R., O’Connor, M., and Rogers, P. Creating the first confidential gpus. *Commun. ACM*, 67(1):60–67, dec 2023. ISSN 0001-0782. doi: 10.1145/3626827. URL <https://doi.org/10.1145/3626827>.
- Fang, C., Jia, H., Thudi, A., Yaghini, M., Choquette-Choo, C. A., Dullerud, N., Chandrasekaran, V., and Papernot, N. Proof-of-learning is currently more broken than you think, 2023.
- Garg, S., Goel, A., Jha, S., Mahlouiifar, S., Mahmood, M., Policharla, G.-V., and Wang, M. Experimenting with zero-knowledge proofs of training. Cryptology ePrint Archive, Paper 2023/1345, 2023. URL <https://eprint.iacr.org/2023/1345>. <https://eprint.iacr.org/2023/1345>.
- Goldwasser, S., Kim, M. P., Vaikuntanathan, V., and Zamir, O. Planting undetectable backdoors in machine learning models, 2022.
- Gupta, K., Jawalkar, N., Mukherjee, A., Chandran, N., Gupta, D., Panwar, A., and Sharma, R. Sigma: Secure gpt inference with function secret sharing. Cryptology ePrint Archive, Paper 2023/1269, 2023. URL <https://eprint.iacr.org/2023/1269>.

- <https://eprint.iacr.org/2023/1269>. <https://eprint.iacr.org/2023/1269>.
- Hubinger, E., Denison, C., Mu, J., Lambert, M., Tong, M., MacDiarmid, M., Lanham, T., Ziegler, D. M., Maxwell, T., Cheng, N., Jermyn, A., Askill, A., Radhakrishnan, A., Anil, C., Duvenaud, D., Ganguli, D., Barez, F., Clark, J., Ndousse, K., Sachan, K., Sellitto, M., Sharma, M., DasSarma, N., Grosse, R., Kravec, S., Bai, Y., Witten, Z., Favaro, M., Brauner, J., Karnofsky, H., Christiano, P., Bowman, S. R., Graham, L., Kaplan, J., Mindermann, S., Greenblatt, R., Shlegeris, B., Schiefer, N., and Perez, E. Sleeper agents: Training deceptive llms that persist through safety training, 2024.
- Jia, H., Yaghini, M., Choquette-Choo, C. A., Dullerud, N., Thudi, A., Chandrasekaran, V., and Papernot, N. Proof-of-learning: Definitions and practice. *CoRR*, abs/2103.05633, 2021. URL <https://arxiv.org/abs/2103.05633>.
- Jooybar, H., Fung, W. W. L., O’Connor, M., Devietti, J., and Aamodt, T. M. Gpudet: a deterministic gpu architecture. In *ASPLOS ’13: Proceedings of the eighteenth international conference on Architectural support for programming languages and operating systems*, 2013.
- Kahan, W. Further remarks on reducing truncation errors, 1965. URL <https://dl.acm.org/doi/pdf/10.1145/363707.363723>.
- Kang, D., Hashimoto, T., Stoica, I., and Sun, Y. Scaling up trustless dnn inference with zero-knowledge proofs, 2022.
- Koh, P. W., Steinhardt, J., and Liang, P. Stronger data poisoning attacks break data sanitization defenses, 2021.
- Kong, Z., Chowdhury, A. R., and Chaudhuri, K. Can membership inferencing be refuted?, 2023.
- Lee, S., Ko, H., Kim, J., and Oh, H. vcnn: Verifiable convolutional neural network based on zk-snarks. Cryptology ePrint Archive, Paper 2020/584, 2020. URL <https://eprint.iacr.org/2020/584>. <https://eprint.iacr.org/2020/584>.
- Liu, T., Xie, X., and Zhang, Y. zkenn: Zero knowledge proofs for convolutional neural network predictions and accuracy. Cryptology ePrint Archive, Paper 2021/673, 2021. URL <https://eprint.iacr.org/2021/673>. <https://eprint.iacr.org/2021/673>.
- Merkle, R. C. A digital signature based on a conventional encryption function. In Pomerance, C. (ed.), *Advances in Cryptology — CRYPTO ’87*, pp. 369–378, Berlin, Heidelberg, 1988. Springer Berlin Heidelberg. ISBN 978-3-540-48184-3.
- Micali, S. CS proofs (extended abstracts). In *35th Annual Symposium on Foundations of Computer Science, Santa Fe, New Mexico, USA, 20-22 November 1994*, pp. 436–453. IEEE Computer Society, 1994. doi: 10.1109/SFCS.1994.365746. URL <https://doi.org/10.1109/SFCS.1994.365746>.
- Nilsson, A., Bideh, P. N., and Brorsson, J. A survey of published attacks on intel sgx, 2020.
- NVIDIA. Determinism across gpu architectures, 2022. URL <https://github.com/NVIDIA/framework-reproducibility/issues/28>.
- NVIDIA. Cuda: Hopper tuning guide, 2023. URL https://docs.nvidia.com/cuda/pdf/Hopper_Tuning_Guide.pdf.
- Sevilla, J., Heim, L., Ho, A., Besiroglu, T., Hobbhahn, M., and Villalobos, P. Compute trends across three eras of machine learning. In *2022 International Joint Conference on Neural Networks (IJCNN)*. IEEE, July 2022. doi: 10.1109/ijcnn55064.2022.9891914. URL <http://dx.doi.org/10.1109/IJCNN55064.2022.9891914>.
- Simonyan, K. and Zisserman, A. Very deep convolutional networks for large-scale image recognition, 2015.
- Srivastava, M., Nushi, B., Kamar, E., Shah, S., and Horvitz, E. An empirical analysis of backward compatibility in machine learning systems, 2020.
- Sun, W., Li, A., Geng, T., Stuijk, S., and Corporaal, H. Dissecting tensor cores via microbenchmarks: Latency, throughput and numeric behaviors, 2022. URL <https://arxiv.org/pdf/2206.02874.pdf#:~:text=Unlike%20Volta%20and%20Turing%20Architecture,%C3%974%C3%978%20MM>.
- TensorFlow. Tensorflow 2.8.0-rc0, 2021. URL <https://github.com/tensorflow/tensorflow/releases/tag/v2.8.0-rc0>.
- Teutsch, J. and Reitwießner, C. A scalable verification solution for blockchains. *CoRR*, abs/1908.04756, 2019. URL <http://arxiv.org/abs/1908.04756>.
- Thudi, A., Jia, H., Shumailov, I., and Papernot, N. On the necessity of auditable algorithmic definitions for machine unlearning. In *31st USENIX Security Symposium (USENIX Security 22)*, pp. 4007–4022, Boston, MA, August 2022. USENIX Association. ISBN 978-1-939133-31-1. URL <https://www.usenix.org/conference/usenixsecurity22/presentation/thudi>.

Wan, A., Wallace, E., Shen, S., and Klein, D. Poisoning language models during instruction tuning, 2023.

Whitehead, N. and Fit-Florea, A. Precision & performance: Floating point and ieee 754 compliance for nvidia gpus, 2011. URL <https://developer.nvidia.com/sites/default/files/akamai/cuda/files/NVIDIA-CUDA-Floating-Point.pdf>.

Zhuang, D., Zhang, X., Song, S. L., and Hooker, S. Randomness in neural network training: Characterizing the impact of tooling. In *arXiv:2106.11872v1*, 2021.

A. GPU Details

All experiments reported in our paper are run with the following three GPUs:

- NVIDIA Titan XP: 3840 Cores, 12 GB
- NVIDIA RTX 2080 Ti: 4352 Cores, 11 GB
- NVIDIA A40: 10752 Cores, 48 GB

We are able to successfully replicate training runs between all pairs of these 3 GPUs.

B. Audit Algorithm

See Algorithm 3.

C. Adaptive Thresholding Algorithm

See Algorithm 4.

D. Time Requirements

See Table 5.

E. Random Number Generation

Our verifiable training scheme requires shared randomness between the trainer and auditor, which is used for deciding input data ordering and batching, weight initialization, and operations such as dropout (randomly setting outputs to zero). More formally, our scheme requires sharing the same random seed and pseudo-random generator. However, in our implementation based on `pytorch` (assuming the same software version between trainer and auditor), we chose to rely on the `torch` random seed functionality. While this successfully controls for batch input ordering and weight initialization, it is unfortunately not sufficient for random number generation, as operations such as `torch.nn.randn()` leverage parallelism when the requested number of values is higher than a certain amount. Specifically, we found that across T40, RTX 2080 Ti, V100, A40, and A100, given the same seed, `torch.randint()` pro-

Table 5. Training time requirements, including Merkle tree operations (at $k = 5$), for 1 step of training broken down by stage of our verifiable training process. Note that reported times are specific to the particular dataset, batch size, and task, and using a non-optimized prototype codebase – therefore the relative increase in time is more important.

| | ResNet-50 | GPT-2 |
|------------------------------------|-----------|-------|
| Original (No Rounding or Disk I/O) | 24s | 8s |
| Trainer | 28s | 11s |
| Auditor | 31s | 13.5 |

duces identical tensors only up to size 40960. At size 40961, T40 (which is an older GPU) deviated from the rest. Likewise, at size 69633, 2080 Ti deviated from the rest, and so on. Based on these observations, we arranged for calls to `torch.randint()` in the dropout layer (which is the only operation using large random tensors in our tasks) to be replaced by generating and concatenating multiple random tensors of size 40960 or less. Specifically, a random tensor of size $n > 40960$ is generated by concatenating $(n // 40960)$ random tensors of size 40960 and one random tensor of size $(n \% 40960)$. However, we emphasize that it is therefore important in our scheme either for both parties to implement this change a priori, or simply use an external source for pseudorandomness.

Algorithm 3 audit

INPUT: dataset D , epochs E , batch size B , shared randomness R , model W_θ , loss function loss , rounding amount b_r , training precision b_{tr} , target model precision b_m , checkpointing interval k , log file F from trainer
 OUTPUT: Merkle tree root M_{root}

```

1:  $M_{leaves} \leftarrow$  create empty leaf list
2:  $W_\theta \leftarrow \text{init}(R, b_{tr})$  // initialize weights
3:  $T \leftarrow \frac{D \cdot E}{B}$ 
4: for  $t = 1 \dots T$  do
5:    $\text{input} \leftarrow \text{batch}(R, D, B)$  // get data batch
   // forward pass
6:   for layer  $l_\theta \in W_\theta.\text{layers}$  do
7:      $\text{output} \leftarrow l_\theta(\text{input})$ 
8:     for  $\text{output}_i \in \text{output}$  do
9:       // Match trainer rounding
10:       $c \leftarrow \text{read}(\text{output}_i, F)$ 
11:       $\text{output}_i \leftarrow \text{rev}(\text{output}_i, b_r, c)$ 
12:    end for
13:     $\text{input} \leftarrow \text{output}$ 
14:  end for
15:   $\text{loss} \leftarrow \text{loss}(\text{output})$ 
16:  // backward pass
17:   $\text{grad\_output} \leftarrow \nabla_{\text{loss}}$ 
18:  for layer  $l_\theta \in W_\theta.\text{layers}$  do
19:     $\text{grad\_input} \leftarrow \nabla_{l_\theta}(\text{grad\_output})$ 
20:    for  $\text{grad\_input}_i \in \text{grad\_input}$  do
21:      // Match trainer rounding
22:       $c \leftarrow \text{read}(\text{grad\_input}_i, F)$ 
23:       $\text{grad\_input}_i \leftarrow \text{rev}(\text{grad\_input}_i, b_r, c)$ 
24:    end for
25:     $\text{grad\_output} \leftarrow \text{grad\_input}$ 
26:  end for
27:   $\theta \leftarrow \text{update\_update\_weights}$ 
28:  if  $t \bmod k = 0$  then
29:     $M_{leaves}.\text{append}(\text{hash}_{\text{sha256}}(\theta \text{ in precision } b_m))$ 
30:  end if
31: end for
32:  $M_{root} \leftarrow \text{tree}(M_{leaves})$  // create Merkle tree
33: return  $M_{root}$ 

```

Algorithm 4 threshold

INPUT: layer l , rounding amount b_r , training precision b_{tr}
 OUTPUT: threshold τ

```

1:  $P \leftarrow$  initialize empty list
2:  $N, T \leftarrow$  initialize large number of data points and iterations
3: for  $i = 1 \dots N$  do
4:    $\text{GPU1}, \text{GPU2} \leftarrow$  select two different GPU architectures
5:    $x \leftarrow$  select random input for layer  $l$  in  $b_{tr}$  floating point precision
6:    $y_1 \leftarrow l_{\text{GPU1}}(x), y_2 \leftarrow l_{\text{GPU2}}(x)$ , apply layer  $l$  on input  $x$  on each GPU
7:   if  $\text{rnd}_{b_r}(y_1) \neq \text{rnd}_{b_r}(y_2)$  then
8:     if  $y_1 > \text{rnd}_{b_r}(y_1)$  and  $y_2 < \text{rnd}_{b_r}(y_2)$  then
9:        $P.\text{append}(|y_1 - \text{rnd}_{b_r}(y_1)|)$ 
10:       $P.\text{append}(|y_2 - \text{rnd}_{b_r}(y_2)|)$ 
11:     end if
12:     if  $y_1 < \text{rnd}_{b_r}(y_1)$  and  $y_2 > \text{rnd}_{b_r}(y_2)$  then
13:        $P.\text{append}(|y_1 - \text{rnd}_{b_r}(y_1)|)$ 
14:        $P.\text{append}(|y_2 - \text{rnd}_{b_r}(y_2)|)$ 
15:     end if
16:   end if
17: end for
18: //binary search to select threshold
19:  $\text{lower}, \text{upper}, \tau \leftarrow 0.25 * (2^{-23}), 0.5 * (2^{9-b_r}), 0$ 
20: for  $t = 1 \dots T$  do
21:    $\tau \leftarrow (\text{lower} + \text{upper})/2$ 
22:    $\text{success} \leftarrow \text{True}$ 
23:   for  $p_i \in P$  do
24:      $\text{exp} \leftarrow$  get exponent of  $p_i$ 
25:     if  $p_i < \text{exp} * \tau$  then
26:        $\text{success} \leftarrow \text{False}$ 
27:     end if
28:   end for
29:   if  $\text{success}$  then
30:      $\text{lower} \leftarrow \tau$ 
31:   else
32:      $\text{upper} \leftarrow \tau$ 
33:   end if
34: end for
35: return  $\tau$ 

```
